Secondary Structure and Interaction of Phage D108 Ner Repressor with a 61-Base-Pair Operator: Evidence for Altered Protein and DNA Structures in the Complex†

James M. Benevides,‡ George Kukolj,§,‖ Chantal Autexier,§,⊥ Kelly L. Aubrey,‡ Michael S. DuBow,§ and George J. Thomas, Jr.*,‡

Division of Cell Biology and Biophysics, School of Biological Science, University of Missouri—Kansas City, Kansas City, Missouri 64110, and Department of Microbiology and Immunology, McGill University, Montréal, Québec, Canada H3A 2B4

Received January 26, 1994; Revised Manuscript Received June 23, 1994®

ABSTRACT: Ner repressors of the transposable phages Mu and D108 play a central role in regulating the expression of the early (transposase) operon and in ensuring that phage growth proceeds along a lytic pathway. The latter function is analogous to that performed by the Cro protein of phage λ. Unlike λ Cro, however, the structural basis of operator recognition is not known for the Ner repressors. In order to elucidate the structural features underlying operator recognition by Ner repressors, we have employed Raman spectroscopy as a probe of the solution secondary structures of both D108 Ner and Mu Ner. Additionally, we have obtained Raman spectra of the D108 Ner repressor when bound to a 61-base-pair oligodeoxynucleotide containing the 55-base-pair D108 *ner* binding site. Conformation-sensitive Raman bands show that both D108 and Mu Ner contain similar, highly α-helical (≈45%) secondary structures. The Raman markers also show that the substantial nonhelical secondary structure of both D108 Ner and Mu Ner is largely β-stranded. The protein-free 61-bp D108 *ner* operator exhibits Raman marker bands diagnostic of an uninterrupted B DNA duplex. In the D108 Ner:DNA complex, we find the following: (i) B DNA stereochemistry is fully conserved, although with significant perturbations to the B form backbone geometry, particularly in AT-rich regions of the bound operator. (ii) The specific interactions that occur between Ner repressor and operator involve B DNA major groove sites. (iii) A small (8 ± 3%) increase in α-helix content of the Ner repressor is detected upon operator binding. (iv) Finally, the local environments of many aromatic amino acids are substantially altered in the D108 Ner:DNA complex. We propose a molecular model for binding of D108 Ner to its operator that is consistent with both the present spectroscopic findings and the results of recent biochemical studies. Essential features of this model are bending of the DNA double helix and contact of operator sites with repressor domains bearing sequence homologies with the helix–turn–helix (HTH) motifs of other DNA-binding proteins. The Raman fingerprint of the Ner:DNA complex is shown to be clearly distinguishable from that of the λ cI:DNA complex, even though both gene regulatory complexes are presumed to employ HTH recognition motifs. The unique Raman signatures observed for these repressor complexes suggest that the Raman methodology may be useful in discriminating different modes of operator recognition by the HTH motifs of regulatory proteins.

The Ner protein from the temperate bacteriophage D108 contains 73 amino acids, which share approximately 50% homology with the 75 amino acids of the Ner protein from the related bacteriophage Mu (Tolias & DuBow, 1985). Together with host proteins, the Ner and c repressors of these bacteriophages determine whether phage growth proceeds, respectively, along a lytic or lysogenic pathway in a manner functionally analogous to that of the well-characterized Cro and cI proteins of bacteriophage λ [for reviews, see Harshey (1988) and Pato (1989)]. However, unlike the well-characterized bacteriophage λ proteins, which employ the helix–turn–helix (HTH) motif as a key recognition element, little is known of the specific recognition mechanism employed by Ner in operator discrimination.

The D108 *ner* operator contains two perfect 11-bp inverted repeats separated by an 8-bp AT-rich domain. Results of chemical and enzymatic protection experiments suggest that D108 Ner makes base-specific contacts in the major groove spanning these 11-bp repeats. Nonspecific protection extends outside this region to encompass, in total, five turns of the DNA double helix (Kukolj et al., 1989a). Although D108 Ner exists in solution as a monomer, even at relatively high concentrations (>5 μM) it appears to bind cooperatively as a dimer to its operator site. Apparently, D108 Ner interacts with its operator in a significantly different manner than does Cro, which forms a dimer in the absence of DNA and makes base-specific contacts over a region encompassing less than two turns of the double helix.

High-resolution structures of several DNA-binding proteins have been determined [for reviews, see Steitz (1990) and Harrison and Aggarwal (1990)]. The results indicate that a

† Paper LI in the series Raman Spectral Studies of Nucleic Acids. Support of this research by the U.S. National Institutes of Health (Grant AI18758) and the Medical Research Council of Canada (Grant MT6751) is gratefully acknowledged. C.A. was supported by a postgraduate scholarship from the Natural Sciences and Engineering Research Council (NSERC) of Canada and a studentship from the Fonds de la Recherche en Santé du Québec (FRSQ). G.K. was supported by a postgraduate studentship from the Fonds pour la Formation de Chercheurs et l'Aide à la Recherche (FCAR). M.S.D. is a Research Scholar (Exceptional Merit) of the Fonds de la Recherche en Santé du Québec (FRSQ).

* Author to whom correspondence may be addressed.
‡ University of Missouri—Kansas City.
§ McGill University.
‖ Present address: Fox Chase Cancer Center, Philadelphia, PA 19111.
⊥ Present address: Cold Spring Harbor Laboratory, Cold Spring Harbor, NY 11724.

® Abstract published in *Advance ACS Abstracts,* August 1, 1994.

0006-2960/94/0433-10701$04.50/0

variety of structural frameworks can be utilized in DNA recognition. On the basis of chemical and enzymatic protection experiments (Kukolj et al., 1989a), the DNA-binding characteristics exhibited by D108 Ner are not consistent with any known DNA-binding motif. Ner may therefore constitute a new member of the diverse and expanding group of protein structural motifs utilized for DNA binding. This idea is supported by recent experiments on Ner homologues in Gram-negative bacteria (Autexier & DuBow, 1992) and humans (Garcia et al., 1992). Although the crystal structures of D108 Ner and Mu Ner have not been solved, the solution structure of Mu Ner has been probed by 2D NMR methods (Gronenborn et al., 1989). The NMR results have been interpreted in terms of a highly α-helical protein, consisting of five helices with no apparent β-sheet structure. The NMR solution conformation has been regarded by Gronenborn et al. (1989) as being more similar in its secondary structure content to the DNA-binding domain of λ repressor (Pabo & Lewis, 1982; Jordan & Pabo, 1988) than to that of λ Cro (Anderson et al., 1981).

If the polypeptide fold of D108 Ner is similar to that of either λ repressor or λ Cro, it remains to be determined how the protein forms contacts over the five turns of its operator double helix. To address this question, we have employed laser Raman spectroscopy as a probe of the solution secondary structures of the Ner protein, the *ner* operator, and their complex. Raman measurements have been performed on both D108 Ner and Mu Ner, and we have compared the solution structure of D108 Ner in the absence of operator DNA with its structure in the presence of a 61-bp oligonucleotide containing the 55-bp D108 *ner* operator sequence. The present results demonstrate both similarities and differences in the conformations of D108 Ner and Mu Ner in solution and help to define the limits of secondary structure homology with λ repressor and λ Cro. We present evidence that the solution conformations of both the D108 Ner repressor and the *ner* operator are significantly altered upon interaction with one another. The structural perturbations attendant with formation of the D108 Ner:DNA complex are distinctly different from perturbations observed in the λ cI:O_L1 complex, which have been investigated previously by Raman spectroscopy (Benevides et al., 1991a,b, 1994). We propose a structural model for D108 Ner:DNA that accounts for both the spectroscopic and biochemical properties of the nucleoprotein complex. We also note the feasibility of Raman spectroscopy as a probe of the protein-induced bending of DNA.

MATERIALS AND METHODS

1. Preparation and Purification of Ner Proteins. D108 and Mu Ner were overexpressed in *Escherichia coli* strain NF1 (λ $cI_{857}N_{am7am53}$) under the control of the λ P_L promoter in plasmids pPLDner and pLMN10, respectively. Plasmid pPLDner contains the 262-bp *HinfI*/*AccI* *ner* gene-containing restriction fragment of the D108 genome (Mizuuchi et al., 1986) in the expression vector pPLEX (Sczakiel et al., 1987). Plasmid pLMN10 harbors the 281-bp *MnlI*/*HinfI* *ner*-encoding restriction fragment from Mu (Priess et al., 1982) in plasmid pPLEX. *E. coli* LF7064 and LF119 are derivatives of NF1-containing recombinant plasmids pPLDner and pLMN10, respectively.

Strains LF7064 and LF119 served as the source of the purification of D108 Ner and Mu Ner, respectively. The activities of the Ner proteins were monitored using the operator binding assay (Kukolj et al., 1989a,b). Proteins were visualized by electrophoresis in 20% Giulian SDS–PAGE[1] gels (Giulian et al., 1985) and stained with silver as described by Morrisey (1981). Protein concentrations were determined using calculated molar extinction coefficients at 280 nm of 2.1×10^4 M^{-1} cm^{-1} for Mu Ner and 1.5×10^4 M^{-1} cm^{-1} for D108 Ner.

Purification was performed as previously described for Mu Ner (Allet et al., 1988), but with the modifications described below. The buffers used in protein purification were as follows: buffer A, 25 mM Tris-HCl (pH 7.8), 250 mM sucrose, and 1 mM PMSF (Sigma); buffer B, 50 mM Tris-HCl (pH 7.8), 2.0 mM EDTA, 1 mM PMSF, and 0.5 mM DTT; buffer C, 50 mM Tris-HCl (pH 7.8), 1 mM EDTA, 5% (v/v) glycerol, and 0.5 mM DTT; buffer D, 50 mM sodium phosphate (pH 7.0), 0.5 mM EDTA, 5% (v/v) glycerol, and 0.5 mM DTT; buffer E, 100 mM Tris-HCl (pH 7.5), 0.5 mM EDTA, 5% (v/v) glycerol, and 0.5 mM DTT.

Cells were grown in 18-L cultures at 32 °C to an A_{550} of 0.6; the temperature was then raised to 42 °C until the A_{550} reached 1.5. Cells were harvested by centrifugation at 5000*g* for 15 min, and the pellets (96 and 55 g of wet weight for LF7064 and LF119, respectively) were stored at −20 °C. All subsequent purification steps were performed at 4 °C. LF7064 frozen cells were thawed and washed in 500 mL of buffer A and collected by centrifugation at 10000*g* for 30 min. The pelleted cells were resuspended with 150 mL of buffer B and passed through a French pressure cell at 124 MPa (18 000 lb/in.^{2}). The suspension was subjected to centrifugation at 10000*g* for 30 min, and the resultant supernatant fluid was centrifuged at 60000*g* for 60 min. The supernatant fluid was dialyzed against 4 L of buffer C overnight. A 132-mL volume of crude extract containing 4.2 g of protein was obtained (D108 Ner fraction I).

LF119 frozen cells were lysed in a 400-mL Biospec BEADBEATER metal chamber filled with 1 M NaCl, 1 mM benzamidine (Sigma), 467 μg/mL PMSF, and 200 mL dry volume of sterile glass beads (0.1 mm diameter). Cells were ground discontinuously for 10 min by alternating 1 min on/off cycles. The suspension was subjected to centrifugation at 5000*g* for 15 min, and the resulting pellet was reground and collected as above. The supernatant fluids were combined, clarified by centrifugation at 80000*g* for 2.5 h at 4 °C, and dialyzed extensively as above. A 310-mL volume of crude extract containing 3.9 g of protein was obtained (Mu Ner fraction I).

Fractions I were loaded independently onto DEAE-Sephadex (Pharmacia) columns (4 × 35 cm) equilibrated in buffer C. The columns were washed with buffer C, and Ner-specific DNA-binding activities were eluted in this buffer (D108 Ner: fraction II, 510 mL, 4 g of protein; Mu Ner: fraction II, 1350 mL, 2.6 g of protein). Fractions II were diluted 2-fold with buffer D, and the slightly cloudy solutions were filtered using 0.8 μm pore size nitrocellulose membranes (Millipore filter type AAWP) and applied to CM-Sepharose (Pharmacia) columns (4 × 20 cm) equilibrated in buffer D. Linear gradients of 0–500 mM NaCl in buffer D were applied; D108 Ner was eluted with about 200–300 mM NaCl, and Mu Ner eluted over the range 120–250 mM NaCl.

To the CM-Sepharose pooled fractions III (D108 Ner: 340 mL; Mu Ner: 550 mL) was added solid ammonium sulfate to 3.4 M (87.5% saturation). The precipitates were collected by centrifugation at 10000*g* for 30 min, dissolved in 9 mL (for

[1] Abbreviations: SDS, sodium dodecyl sulfate; PAGE, polyacrylamide gel electrophoresis; EDTA, ethylenediaminetetraacetic acid; Tris-HCl, tris(hydroxymethyl)aminomethane hydrochloride; DTT, dithiothreitol; PMSF, phenylmethanesulfonyl fluoride; HPLC, high-pressure liquid chromatography; DEAE, (diethylamino)ethyl; CM, carboxymethyl; TEA, triethylamineacetate; bp, base pair; MW, molecular weight; CAP, catabolite gene activator protein, also known as cAMP receptor protein (or CRP); HTH, helix–turn–helix.

FIGURE 1: Sequence of the 61-bp DNA (*ner* operator), which contains the D108 Ner-binding site. The 11-bp inverted repeats, which straddle the central eight base pairs of the binding domain, are shown in boldface type.

D108 Ner) or 6 mL (for Mu Ner) of buffer E, filtered with Millex-GV 0.22 μm pore size filter units (Millipore), and applied to Sephadex G-75 superfine (Pharmacia) columns (2.5 × 30 cm) equilibrated in buffer E. The columns were washed with buffer E, and the respective Ner-containing fractions were pooled (fractions IV: D108 Ner, 36 mL, 23 mg; Mu Ner, 25 mL, 7 mg). Fractions IV were loaded onto Heparin Sepharose CL-6B (Pharmacia) columns (1 × 15 cm) equilibrated in buffer E. Linear gradients of 0–600 mM NaCl were applied. D108 Ner eluted in the range 200–300 mM NaCl, and Mu Ner eluted between 135 and 230 mM NaCl. Fractions containing >99% pure Ner were pooled (D108 Ner, 9 mL, 14 mg; Mu Ner, 1.3 mL, 0.7 mg), dialyzed against 7.5 mM Tris-HCl (pH 7.6), concentrated to 2.2 mg/mL (D108 Ner) or 1 mg/mL (Mu Ner), respectively, using a Centricon-3 microconcentrator (Amicon), and stored at 4 °C until use.

2. Synthesis and Purification of D108 ner Operator. D108 *ner* operator (MW 36 500) was synthesized as asymmetric 61-nucleotide oligomers on an Applied Biosystems Model 381A DNA synthesizer using controlled pore glass supports and β-cyanoethyl phosphoramidite derivatives. Its sequence is shown in Figure 1. The D108 Ner-binding site comprises the internal 55 bp in Figure 1. An additional 3 bp, constituting the blunt enzyme site, *Sma*I, was incorporated at each end for future cloning applications. Purification of single strands was performed on an ISCO Model 2350 HPLC system. Details of the instrumentation and purification procedure have been given elsewhere (Benevides et al., 1994). Briefly, the 61-mers were isolated with the terminal trityl groups in place. An initial trityl-on separation was done on a PRP-1 reversed phase column (Hamilton). The mobile phase was as follows: (A) 0.2 M TEA (pH 7.0), (B) distilled water, and (C) acetonitrile (Optima grade, Fisher Scientific). For the elution gradient, A was maintained at 50%, while B and C were mixed to form a linear gradient in which C increased from 5% to 50% over a 45-min time interval. Flow was maintained at 1.0 mL/min. After recovery, each strand was detritylated and rerun on the HPLC system under conditions similar to those used above for the trityl-on separation, except that a linear gradient of C was established that increased from 0% to 25% over a 60-min time interval. The trityl-off separation served to resolve the desired detritylated sequence from undesirable byproducts of the detritylation step.

3. Preparation of D108 ner Operator Duplex. Each strand was resuspended in approximately 2.0 mL of 0.1 M NaCl, pH 7.0. Concentrations were determined from UV absorbance measurements at 260 nm. Equimolar amounts of each strand were mixed and annealed by heating to 90 °C for 15 min in a dry bath, followed by slow cooling. After annealing, the solution was dialyzed for several hours at 5 °C against 2 M NaCl + 1 mM EDTA. Dialysis was continued for an additional 24 h against several changes of distilled water. The duplex solution was lyophilized to near dryness and redissolved at a concentration of 40 μg/μL in 7.5 mM Tris, pH 7.87. The duplex product was verified by HPLC analysis on a hydroxylapatite column (Bio-Rad) and on 15% polyacrylamide gels.

4. Preparation of D108 Ner:DNA Complexes. Protein:DNA complexes were prepared by dissolving the appropriate weight of operator in a solution containing 50 μg/μL D108 Ner protein so as to produce a 4:1 molar ratio of Ner monomer to operator duplex. This was done to ensure that all operator was completely bound by protein. Complex formation was confirmed by gel mobility assays.

5. Raman Spectroscopy. Solutions of Ner proteins, *ner* operator, and complexes were prepared as described above and sealed in glass capillary cells (Kimax no. 34507) thermostated at 12 °C throughout the data collection protocols. All spectra were acquired on a Spex Ramalog V/VI spectrometer under the control of an IBM-XT microcomputer. The 514.5-nm argon line of a Coherent Innova laser was used as the excitation source. Data were collected over the spectral interval 300–1800 cm^{-1} with 1-cm^{-1} increments, an integration time of 1.5 s, and a spectral slit width of 8 cm^{-1}. The Raman spectra over this region presented below are averages of 10–15 scans of 1.5 cm^{-1} or better repeatability. For spectral regions containing the amide I (1500–1750 cm^{-1}) and amide III (1130–1520 cm^{-1}) bands, an additional 20–30 scans were signal averaged to further reduce spectral noise. In all instances, solvent was compensated by computer subtraction techniques described previously (Benevides et al., 1984). Raman frequencies of well-resolved bands are accurate to within ±1.5 cm^{-1}. For the normalization of difference spectra, the Raman band at 1093 cm^{-1}, due to the symmetric P–O stretching vibration of the phosphodioxy group (PO_2^-), was used as an internal intensity standard, as previously described (Benevides et al., 1991a).

We have employed the following criteria for selection and discussion of peaks and troughs in difference spectra. First, a difference feature is deemed to have significant intensity if it reflects *both* a relative intensity change of at least 10% in comparison to its parent bands *and* a signal-to-noise ratio of at least 2:1 in the computed difference spectrum. Second, the difference band must be structurally interpretable. Thus, while a difference band may, in principle, be significant by the first criterion, it may be impossible to interpret in sufficient detail to warrant discussion. However, there are few bands in the present spectra that meet only the first criterion.

Fourier deconvolution was employed to enhance spectral resolution in the Raman amide I region, using a procedure that conserves integrated intensities of the deconvoluted band components (Thomas & Agard, 1984). A Gaussian–Lorentzian product function of 22 cm^{-1} half-width, consistent with the spectrometer slit function (Thomas & Agard, 1984), was used as the desmearing band. The deconvolution results were qualitatively invariant to half-widths between 20 and 24 cm^{-1}, consistent with previous applications to λ repressor (Thomas et al., 1986) and other phage proteins (Sargent et al., 1988). Deconvoluted components obtained with the different desmearing bands exhibited peak heights and apparent areas that differed by less than the limits of uncertainty quoted in the tabulations below (see section 3 of Results and Interpretation). The amide I region was also fit to the minimum number (three) of Gauss–Lorentz curves by a nonlinear least-squares procedure (SpectraCalc), in which the component bandwidths were constrained to 35 ± 2 cm^{-1}. The curve-fitting results could not be improved by either increasing the number of components or altering the component bandwidths, as judged by the χ-values (sum of residuals). Amide I data were convolution smoothed (13-point) before deconvolution or curve fitting. In no case did smoothing significantly change Raman line frequencies or intensities.

Table 1: Selected Raman Conformational Markers of DNA[a]

residue	B DNA	A DNA	Z DNA
G	682 ± 2	664 ± 2	625 ± 3
	1318 ± 2	1333 ± 3	1316 ± 2[b]
A	663 ± 2	644 ± 4	624 ± 3
	1339 ± 2	1335 ± 2	1310 ± 5
C	782 ± 2	780 ± 2	784 ± 2
	1255 ± 5	1252 ± 2	1265 ± 2
T	748 ± 2	745 ± 2	
	790 ± 3	777 ± 2	
	1208 ± 2	1239 ± 2	
backbone	790 ± 5	705 ± 2	745 ± 3
	835 ± 7[c]	807 ± 3[d]	
	1092 ± 1	1099 ± 1	1095 ± 2
	1422 ± 2	1418 ± 2	1425 ± 2

[a] Frequencies in cm^{-1} units are determined from the Raman spectra of DNA crystals and fibers of known structure [see Thomas and Wang (1988) and references therein]. [b] A weak band near 1316 cm^{-1} is also present in B DNA structures. [c] The band center is sensitive to base composition (Benevides et al., 1991c). [d] The corresponding band of RNA occurs at 813 cm^{-1}.

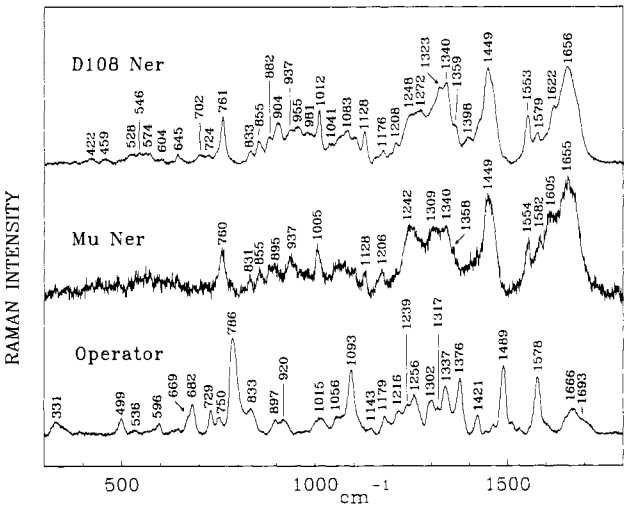

FIGURE 2: Raman spectra in the region 300–1800 cm^{-1} of the D108 *ner* operator (bottom), Mu Ner (middle), and D108 Ner (top). Labels indicate the frequencies in cm^{-1} units of major bands discussed in the text. Conditions: D108 Ner, 60 μg/μL in 7.5 mM Tris, pH 7.5; Mu Ner, 30 μg/μL in 7.5 mM Tris, pH 7.5; *ner* operator, 40 μg/μL in 7.5 mM Tris, pH 7.5. Data are the averages of 8–12 scans collected at 12 °C with an integration time of 1.5 s and a slit width of 8 cm^{-1}.

RESULTS AND INTERPRETATION

Previous Raman studies of nucleic acid crystals and fibers of known conformation (Thomas & Wang, 1988) have established that specific Raman bands are sensitive to changes in phosphodiester torsions and to coupled changes in nucleoside sugar pucker and glycosyl torsion. These bands, which are referred to as backbone conformation markers and nucleoside conformation markers, respectively, are listed in Table 1.

1. Raman Spectrum of ner Operator. The Raman spectrum in the region 300–1800 cm^{-1} of the 61-bp D108 *ner* operator is shown in Figure 2 (bottom). The backbone conformation markers at 833 and 1093 cm^{-1} are typical of B DNA of this base composition (Thomas & Wang, 1988). The nucleoside conformation markers at 682 (dG), 729 (dA) 750 (dT), and 1256 cm^{-1} (dC) identify C′-*endo*/*anti* conformers. The relative intensities of the 682- and 729-cm^{-1} bands are in accord with the base composition of the Figure 1 sequence (54% GC, 46% AT).

2. Raman Spectra of D108 Ner and Mu Ner. The Raman spectra in the region 300–1800 cm^{-1} of D108 Ner and Mu Ner are included in Figure 2. The Raman frequencies, relative intensities, and assignments are summarized in Table 2. The spectra of both D108 Ner (Figure 2, top) and Mu Ner (Figure 2, middle) are dominated by bands originating from modes of the peptide backbone, particularly the amide I (1640–1690 cm^{-1}) and amide III (1245–1320 cm^{-1}) modes, which are diagnostic of the secondary structure. These will be discussed further in sections 3 and 4.

Table 2: Raman Frequencies, Intensities, and Assignments for D108 Ner and Mu Ner Proteins[a]

D108 Ner		Mu Ner		
frequency	intensity	frequency	intensity	assignment[b]
422	0.5			
459	0.5			
528	1.0			W
546	1.2			amide VII
574	1.2			amide VII
604	0.5			M
645	1.0			Y
702	1.0			M; amide V
724	0.9			M
761	5.0	760	3.9	W
833	1.2	831	1.5	Y
855	2.4	855	2.2	Y
882	2.7			W
904	4.2			A
937	3.6	937	3.3	skeletal mode of α-helix
965	3.8			[CH_3 symmetric rock]
981	3.3			I
		1005	4.3	F
1012	5.6			W
1041	2.1			S [C–O stretch]
1083	3.5			
1128	3.3	1128	1.9	W; [C–C stretch]
1176	1.4	1172	2.2	[CH_3 asymmetric rock]
1208	3.3	1206	2.1	Y
1248	5.2	1242	6.1	amide III
1272	5.5			amide III
1323	8.0	1309	5.9	[CH_2 twist/wag]
1340	8.5	1340	6.1	W; [CH_2 twist/wag]
1359	4.1	1358	4.1	W
1398	2.7			CO_2^- symmetric stretch
1449	10.0	1449	8.8	[CH_2 scissor]
1553	5.1	1554	4.7	W
1579	3.3	1582	5.0	W
		1605	7.1	F, Y
1622	6.0			Y, W
1656	10.0	1655	10.0	amide I

[a] Frequencies are in cm^{-1} units, and intensities are based upon a 0–10 scale for bands in the spectra of Figure 2. [b] Bands assigned to the vibrational modes of multiple aliphatic side chains are enclosed in square brackets ([ ]). Other side-chain assignments are indicated using standard notation for the amino acids. Amide modes are discussed in the text. The basis for assignments is given in Thomas et al. (1983) and Aubrey and Thomas (1991).

Other major contributors to the Ner spectra of Figure 2 are Raman bands assigned to CH groups of aliphatic side chains (1449 cm^{-1}), tyrosines (645, 833, 855, 1176, 1208, 1272, and 1622 cm^{-1}), and tryptophans (761, 882, 1012, 1340, 1359, 1553, and 1579 cm^{-1}). Since D108 Ner lacks phenylalanine, the usually prominent marker of the phenyl ring (1002 cm^{-1}) is not observed in the Figure 2 spectrum (top). The absence of phenylalanyl Raman markers from the D108 Ner spectrum confirms the high purity of the protein preparations used in this study.

3. Amide I and Amide III Markers of D108 Ner and Mu Ner. Raman amide I and amide III profiles of D108 Ner and Mu Ner are shown on expanded scales in Figure 3. For comparison, the corresponding spectral data of the λ repressor N-terminal domain (residues 1–102) and the λ Cro repressor are included. When appropriately normalized, the Raman amide bands of Figure 3 may be interpreted to reveal similarities and differences in the solution secondary structures

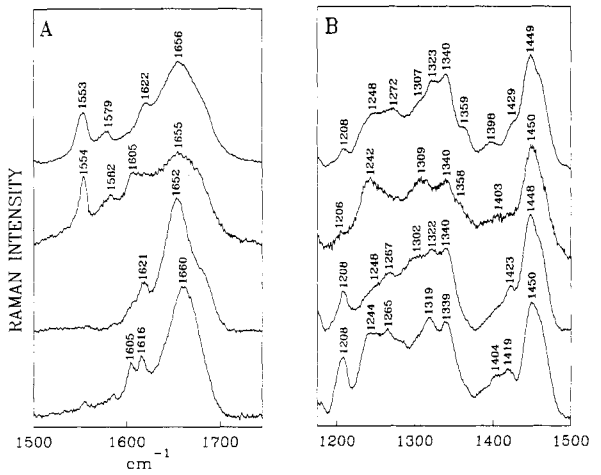

FIGURE 3: From top to bottom: Raman spectra of D108 Ner, Mu Ner, λ repressor N-terminal domain (residues 1–102), and λ Cro repressor. (A) Amide I region (1500–1750 cm^{-1}). (B) Amide III region (1125–1550 cm^{-1}). Conditions: D108 Ner, 60 μg/μL in 7.5 mM Tris, pH 7.5; Mu Ner, 30 μg/μL in 7.5 mM Tris, pH 7.5; λ repressor, 50 μg/μL in 200 mM NaCl, pH 7.8; Cro repressor, 50 μg/μL in 25 mM phosphate + 500 mM KCl, pH 7.0. Data are the averages of 30–50 scans collected under conditions identical to those described in Figure 2.

of these four DNA-binding proteins. For this purpose, we note that the four proteins contain similar aliphatic amino acid compositions. Accordingly, the intense aliphatic CH bending mode near 1450 cm^{-1} in each spectrum of Figure 3B serves as a basis for comparison of the amide III intensities located specifically between 1220 and 1320 cm^{-1}. Similarly, the integrated intensity of the amide I envelope (1640–1700 cm^{-1}) may be used for comparison of the spectral intensities of Figure 3A with one another.

The principal conclusions that can be reached from Figure 3A are as follows. First, the amide I profiles of D108 Ner and Mu Ner are similar to one another. Both exhibit a major peak centered near 1655 cm^{-1}, indicating α-helix as the dominant secondary structure. Second, the α-helix content of each Ner repressor is less than that of the λ repressor N-terminal domain. Third, in all four proteins a shoulder occurs on the high-frequency side of the amide I peak, which is assignable to nonhelical secondary structure. This common feature is least intense for λ repressor (1684-cm^{-1} satellite) and apparently most intense for λ Cro, where it coalesces with the α-helix marker to give a broad composite band centered at ca. 1660 cm^{-1}. Accordingly, the amount of nonhelical secondary structure in each of the Ner proteins is considered to be similar to that observed in λ Cro.

The above conclusions are confirmed by the amide III data of Figure 3B, which further show the following. The nonhelical secondary structures of D108 Ner and Mu Ner are dissimilar. This is evidenced by the fact that in Mu Ner a strong and relatively sharp amide III marker occurs at 1242 cm^{-1}, indicating substantial β-strand structure in this protein (Chen & Lord, 1974). On the other hand, in D108 Ner the amide III satellite occurs at 1248 cm^{-1} and is quite broad, indicating a distribution of nonhelical structural elements, probably including substantial loops and turns as well as β-strand (Chen & Lord, 1974; Thomas et al., 1987). In many respects, the amide III profile of D108 Ner is similar to that of λ repressor, while the amide III profile of Mu Ner is similar to that of λ Cro. Note that the very different aromatic amino acid compositions of the four proteins account for the remaining differences in bands of the spectral region displayed in Figure 3B. For example, both λ and Cro repressors lack tryptophan, which is present in the Ner repressors. The Trp residues of

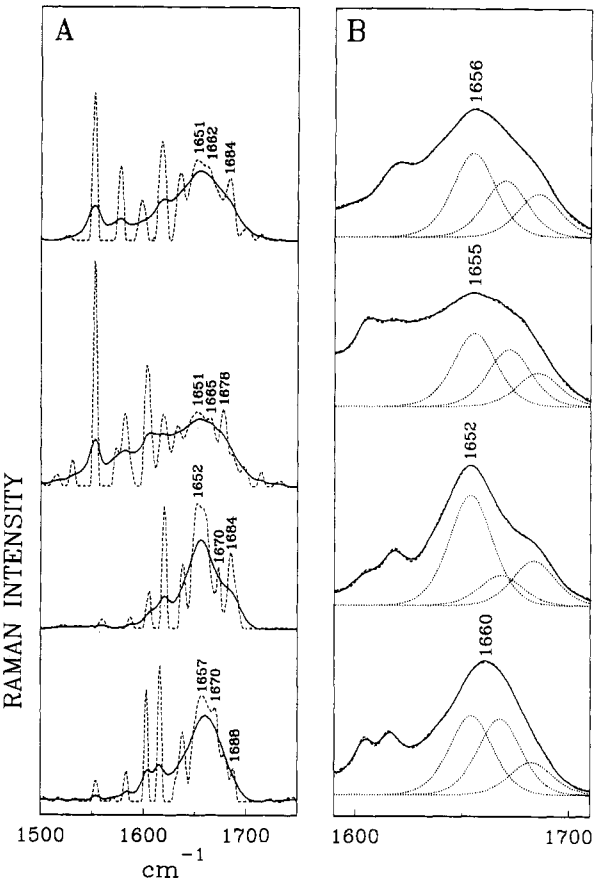

FIGURE 4: From top to bottom: Raman spectra of D108 Ner, Mu Ner, λ repressor N-terminal domain (residues 1–102), and λ Cro repressor. (A) Fourier deconvolution of the amide I region using a Gauss–Lorentz function of 22 cm^{-1} bandwidth. (B) Fitting of the amide I envelope to Gauss–Lorentz (GL) components. Although for clarity of presentation, only the GL components above 1645 cm^{-1} are shown, the entire band envelope was fit with virtually no residuals. The goodness of fit is indicated by the near congruency of the experimental data (solid line) and the sum of components (broken line) throughout the region shown.

D108 Ner (W12 and W69) and Mu Ner (W10, W48, and W67) generate the enhanced intensities near 1340 and 1360 cm^{-1}. Conversely, the Ner repressors have fewer tyrosines. The more prevalent tyrosines of λ and Cro repressors generate enhanced markers near 1208 and 1265 cm^{-1}.

In summary, on the basis of consideration of both amide I and amide III Raman frequencies and intensities, the α-helix contents of the Ner repressors and λ Cro are similar and significantly lower than that of the λ repressor N-terminal domain. The nonhelical segments of D108 Ner and Mu Ner are primarily β-stranded. The amide III data suggest further that the peptide backbone of D108 Ner repressor contains a wider range of ϕ,ψ angles in nonhelical segments than does that of Mu Ner repressor. A larger percentage of turns and loops in D108 Ner repressor is consistent with the Raman spectra.

4. Semiquantitative Estimates of Secondary Structure. The types and amounts of secondary structure present in a protein can be estimated by Fourier deconvolution (Thomas & Agard, 1984) or curve-fitting analysis (Thomas et al., 1987) of the Raman amide I band envelope. Decompositions of the amide I profiles of D108 Ner, Mu Ner, λ repressor, and Cro using both Fourier deconvolution and Gauss–Lorentz (GL) curve-fitting procedures are shown in Figure 4A,B, respectively. A Gaussian desmearing function with full width at half-maximum (FWHM) of 22 cm^{-1} was employed for Fourier deconvolution. GL component bandwidths were restricted to

Table 3: Estimates of Secondary Structure from Raman Amide I Spectra of D108 Ner, Mu Ner, λ Cro, and λ Repressor Proteins

secondary structure type	D108 Ner	Mu Ner	λ Cro[a]	λ repressor[a]
α-helix	46 ± 4	45 ± 4	42 ± 3 (41)	59 ± 5 (64)
β-structure	31 ± 3	34 ± 3	40 ± 3 (30)	16 ± 2
other	24 ± 2	21 ± 2	18 ± 2 (29)	25 ± 2

[a] Values in parentheses are calculated from the corresponding X-ray crystal structures (Jordan & Pabo, 1988; Anderson et al., 1981).

a FWHM of 35 cm^{-1} for bands above 1640 cm^{-1}, and curve fitting was constrained to the minimum number of components, yielding virtual congruency with the experimental data.

The results of Figure 4A suggest multiple overlapping amide I components for each protein, and a simple quantitative interpretation is not feasible. However, in each case the major amide I component occurs near 1654 ± 3 cm^{-1}, diagnostic of α-helix (Chen & Lord, 1974). Further deconvolution (not shown) separates the α-helix component as the principal secondary structure marker of each protein, contributing ≈60% of the total amide I intensity of λ repressor and significantly lesser percentages of the total amide I intensities of D108 Ner (46%), Mu Ner (45%) and Cro (42%).

The curve-fitting results (Figure 4B) also confirm the prevalence of α-helix in each protein. The percentages of amide I intensity contributed by the curve-fitted α-helix markers, interpreted as the percentages of α-helix secondary structure in the proteins, are summarized in Table 3. For λ repressor and λ Cro, the results of Table 3 are consistent with the deconvolution results and are in reasonably good agreement with the available X-ray crystal structures (Pabo & Lewis, 1982; Jordan & Pabo, 1988; Anderson et al., 1981) and NMR solution structure (Bolotina et al., 1983). The three-dimensional structures indicate ≈60% helix in λ repressor and ≈40% helix in λ Cro. The residual amide I intensity in each spectrum of Figure 4B is due to nonhelical structure. The substantial numbers of turns and loops in λ repressor may be represented by the 1684-cm^{-1} amide I component and the substantial β-strand structure of Cro by the 1670-cm^{-1} amide I component. Similarly, the nonhelical structures of Mu (≈55%) and D108 (≈55%) Ner are probably reflected in the amide I components at 1662 and 1665 cm^{-1}, respectively.

The Raman amide band analysis of Mu Ner (Table 3) is in semiquantitative agreement with the recently proposed NMR solution structure (Gronenborn et al., 1989). The only major discrepancy occurs in the question of nonhelical domains of Mu Ner. While the NMR results have been interpreted in terms of ≈65% α-helical structure and essentially no β-strand, the Raman results suggest as much as ≈55% nonhelical structure, probably including substantial β-strands. These findings are further discussed below.

5. Side-Chain Environments. (a) Tyrosine. The ratio of intensities (I_{855}/I_{833}) of the tyrosine Fermi doublet, with components near 855 and 833 cm^{-1}, is diagnostic of the average hydrogen-bonding states of tyrosine phenolic groups (Siamwiza et al., 1975). For the two tyrosines of D108 Ner (Y50 and Y73), I_{855}/I_{833} = 1.87 ± 0.05 (Figure 2), indicating that the two phenoxyls cannot participate as both donors and acceptors of hydrogen bonding, and therefore Y50 and Y73 cannot both be exposed to combined donor and acceptor interactions with solvent H_2O molecules. The simplest interpretation of the data is that one tyrosine is the acceptor of a strong hydrogen bond from a highly positive donor (for which I_{855}/I_{833} = 2.50) and the other is solvent exposed (for which I_{855}/I_{833} = 1.25), thus accounting for an average Fermi doublet intensity ratio of 1.87. Because of the location of Y73 at the C-terminus, we assign it as the solvent-exposed tyrosine. The observed tyrosine doublet intensity ratio would also be consistent with a repressor structure in which both Y50 and Y73 are acceptors of relatively strong hydrogen bonds.

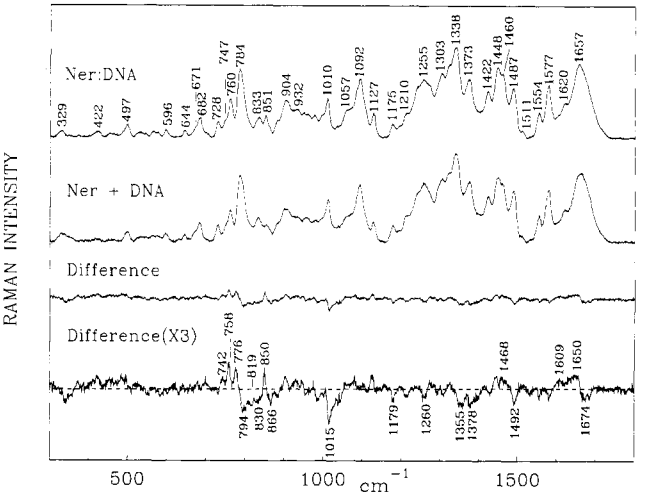

FIGURE 5: Raman spectra in the region 300–1800 cm^{-1} of D108 Ner:DNA complex (top), the sum of constituents (second from top), the difference spectrum (second from bottom), and a 3-fold amplification of the difference spectrum (bottom).

In the case of Mu Ner, the Fermi doublet intensity ratio is less accurately measured ($I_{855}/I_{833} \approx 1.6$; Figure 2). However, the data again suggest that the two tyrosine phenoxyls (Y35 and Y71) function on average more as hydrogen bond acceptors than donors.

(b) Tryptophan. The tryptophan indole ring mode near 875–883 cm^{-1} is diagnostic of the hydrogen-bonding strength of the exocyclic 1NH donor (Miura et al., 1988, 1989). The corresponding band of D108 Ner is observed at 882 cm^{-1} (Figure 2), which is close to its high-frequency limit and indicative of very weak hydrogen bonding by 1NH donors of both W12 and W69.

The tryptophan indole ring also exhibits a Fermi doublet with components near 1360 and 1340 cm^{-1}, the intensity ratio of which is diagnostic of the hydropathicity of the ring environment (Harada et al., 1986) and a ring mode near 1550 cm^{-1}, which is sensitive to the magnitude of the side-chain torsion angle, $|\chi^{2,1}|$ (Miura et al., 1989). The present results (Figure 2) indicate that the average indole ring environment is relatively hydrophilic and that both tryptophans are configured with $|\chi^{2,1}| \approx 102°$.

6. Raman Spectrum of a D108 Ner:DNA Complex. Figure 5 shows the Raman spectrum of the D108 Ner:DNA complex (top) and the spectral sum of its constituents (second from top). Also shown is the difference spectrum (second from bottom) corresponding to the complex minus the sum of its constituents. The prominent difference bands are labeled in the amplified difference spectrum (bottom).

Comparison of the labeled difference bands of Figure 5 with Figure 2 and Table 2 indicates that most are not ascribable to the D108 Ner repressor. Accordingly, most of the structural perturbations attendant with complex formation occur in the *ner* operator DNA. Many of the difference bands are directly assignable to DNA residues by analogy with model compounds (Figure 2 and Table 1) and thus provide information about the nature of the DNA conformational changes that accompany binding of D108 Ner. These are discussed below.

(a) Changes in DNA Structure with Binding of D108 Ner Repressor. (i) Backbone. In the D108 Ner:DNA complex, the Raman intensities in the interval 785–845 cm^{-1} are

significantly reduced in comparison to those in the constituent spectra. This results in negative difference bands with troughs near 794, 819, and 830 cm^{-1} (Figure 5, bottom). An additional trough appears at 866 cm^{-1}. The 794-, 819-, and 866-cm^{-1} troughs are unambiguously assignable to DNA (Small & Peticolas, 1971; Prescott et al., 1984) and indicate structural perturbations to the B DNA backbone induced by Ner binding. Similarly, the difference peaks at 742 and 776 cm^{-1} are assignable to DNA structural perturbations resulting from Ner binding. The trough near 830 cm^{-1}, as well as the peak near 850 cm^{-1}, are assigned predominantly to DNA, despite the expectation of overlapping bands from tyrosine, for the following reason. If the observed difference bands were due to Ner tyrosines, an increase in phenolic OH acceptor hydrogen bonding would be required (Siamwiza et al., 1975). In such a case, the magnitudes of intensity changes at 830 and 850 cm^{-1} would be much smaller than those observed. Accordingly, the 830-cm^{-1} trough and 850-cm^{-1} peak in the Figure 5 difference spectrum must be due predominantly to a change in DNA backbone structure. Finally, as noted below, the 794- and 830-cm^{-1} bands of DNA are interrelated. Both are due to vibrations localized in the phosphodiester groups of B form DNA (Small & Peticolas, 1971; Prescott et al., 1984), and it is expected that both would suffer a parallel intensity change with Ner binding (Benevides et al., 1991c).

The absence of spectral differences in the interval 600–700 cm^{-1} indicates that nucleoside conformations are not altered by the perturbations to B DNA phosphodiester geometry. Clearly, there is no evidence in the Figure 5 difference spectrum of alternative double-helical forms of DNA, such as A DNA or Z DNA.

Previous studies show that Raman intensity decreases at 794 and 830 cm^{-1} and an intensity increase at 776 cm^{-1} accompany changes in B DNA backbone geometry (Erfurth & Peticolas, 1975; Benevides et al., 1991c). The similar spectral features in the D108 Ner:DNA complex (Figure 5) indicate that structural changes are induced in the DNA backbone by Ner binding. Unfortunately, the Raman spectra do not provide further details of the structural changes induced in the DNA backbone by Ner binding, and several possibilities are consistent with the Raman data. Among those observed in other specific protein:DNA complexes, which could account for the Raman results, are changes in DNA winding angles in the *EcoRI* (McClarin et al., 1986) and DNase I complexes (Lahm & Suck, 1991), changes in the roll angles in the catabolite gene activator protein (CAP or CRP) complex (Schultz et al., 1991), and induction of DNA bending in several prokaryotic gene regulatory protein complexes (Koudelka, 1991; Kosturko et al., 1989; Schumacher et al., 1989; Brennan et al., 1990; Schultz et al., 1991).

A decrease in the DNA winding angle leads to a widened major groove, which should enhance the accessibility of hydrogen bond donor and acceptor sites of the bases to solvent and protein groups (McClarin et al., 1986). In A DNA crystal structures, underwinding causes the torsions α and ζ (P–O5′–C5′–C4′ network) at purine–pyrimidine steps to deviate from the usual g^-,g^+ conformation to a t,t conformation (Heinemann et al., 1987). Olson (1982) has suggested that correlated rotations of these torsions from the preferred g^-,g^+ conformation to the t,t conformation may also lead to opening of the B DNA helix. Nucleic acids in which the ζ torsion assumes the *trans* conformation have been studied previously by Raman spectroscopy. The *trans* conformer produces a Raman band in the interval 850–870 cm^{-1} (Nishimura & Tsuboi, 1986; Benevides et al., 1986, 1991a,b). The difference spectrum of Figure 5 reveals an enhanced 850-cm^{-1} band in the complex, which is consistent with *trans* conformers and underwinding of the double helix.

(ii) Bases. Changes in DNA backbone torsions are expected to alter base-stacking geometry. Accordingly, the many additional peaks and troughs throughout the Figure 5 difference spectrum are consistent with alterations in base stacking in the protein-free operator.

The interval 1350–1750 cm^{-1} contains Raman bands that are sensitive to specific interactions between DNA bases and major-groove-binding proteins. Principal among these Raman markers of DNA:protein interactions is the band of dG near 1490 cm^{-1}, which shifts to ca. 1470 cm^{-1} upon hydrogen bond donation to the guanine ring 7N acceptor (Hartman et al., 1973; Nishimura et al., 1986; Benevides et al., 1991a,b, 1994). The difference spectrum of Figure 5 shows a derivative feature with a negative lobe at 1492 cm^{-1} and a positive lobe near 1468 cm^{-1}. This difference feature is assigned to a change in the hydrogen-bonding state of guanine 7N acceptors with the binding of D108 Ner. We conclude that Ner repressor side chains interact with the major groove of the *ner* operator. This is consistent with the mode of DNA interaction of the λ and 434 repressor helix–turn–helix (HTH) domains (Jordan & Pabo, 1988; Clarke et al., 1991; Beamer & Pabo, 1992).

Hydrophobic interaction between a thymine 5-CH_3 group and an aliphatic side chain is expected to result in a Raman intensity increase at 1376 cm^{-1} (Benevides et al., 1991a,b). In the D108 Ner:DNA complex, this intensity actually decreases, as evidenced by the negative difference band at 1378 cm^{-1} (Figure 5). This suggests that, on average, the thymine 5-CH_3 groups of the D108 Ner:DNA complex are less shielded from solvent than those of the protein-free *ner* operator.

Another dissimilarity between the Raman spectrum of the D108 Ner:DNA complex and that of the λ repressor–operator complex occurs in the region 1700–1725 cm^{-1}. In the Figure 5 difference spectrum, no Raman difference band is observed above 1700 cm^{-1}. However, in the λ repressor–operator complex, a characteristic difference feature at 1717 cm^{-1} was attributed to a specific repressor side-chain interaction with the guanine 6-C=O acceptor groups of the operator (Benevides et al., 1991a,b).

(iii) DNA Tertiary Structure. The evidence noted above for alterations in DNA backbone torsions and base-stacking geometry, and particularly for significant perturbations to AT-rich regions of the operator, are consistent with a major change in DNA tertiary structure accompanying the binding of D108 Ner. Specifically, we note that the dominant intensity changes observed at 742 and 1378 cm^{-1} are assignable to thymidine and that the intensity change observed at 819 cm^{-1} is correlated with AT-rich regions of B DNA (Thomas & Peticolas, 1983; Wartell & Harrell, 1986). Although the Raman spectral indicators cannot be interpreted unambiguously in terms of tertiary structure, they suggest changes in B DNA that are consistent with bending of the double helix.

(b) Changes in Ner Conformation with Binding to DNA. The positive band at 1650 cm^{-1} and the negative band at 1674 cm^{-1} in the difference spectrum of Figure 5 indicate that Ner undergoes a small β-strand to α-helix transition with complex formation. The positive difference band at 937 cm^{-1} is also evidence of greater α-helicity (Sengupta & Krimm, 1987) in the complex. The increase in helix, estimated from the amide I intensity change, is 8% ± 3%.

Although the majority of bands in the difference spectrum of Figure 5 are assignable to DNA, several protein Raman bands are also affected by complex formation. The tryptophan markers at 758, 1015, and 1340–1360 cm^{-1} and tyrosine

markers at 1179 and 1609 cm^{-1} show relatively large intensity changes, indicative of altered ring environments in the D108 Ner:DNA complex. The intensity decrease near 1360 cm^{-1} and corresponding increase near 1340 cm^{-1} (Figure 5) reflect greater hydrophilicity for the environment of the average indole ring in the complex.

DISCUSSION AND CONCLUSIONS

1. Ner Secondary Structure. The Raman spectra of D108 Ner and Mu Ner indicate solution secondary structures that contain similar percentages of α-helix. However, both of the Ner repressors exhibit a much broader amide I band than is observed for the N-terminal domain (1–102) of λ cI repressor, indicating that the Ner repressors are not as extensively α-helical as the λ repressor DNA-binding domain. The Raman amide III data further indicate that the nonhelical secondary structure in Ner repressors is largely β-stranded, with D108 Ner apparently containing a broader distribution of nonhelical chain conformations.

The present structural conclusions regarding Mu Ner are qualitatively consistent with the preliminary solution structure proposed on the basis of 2D NMR spectroscopy (Gronenborn et al., 1989). The key point of agreement between Raman and NMR results is the highly α-helical solution structure of Ner repressors. On the other hand, Gronenborn et al. (1989) suggest a greater percentage of α-helix than indicated by the Raman amide band patterns. One explanation for this apparent difference may be the inequivalent sampling conditions used in the two studies. Raman spectroscopy requires solution concentrations (>50 mg/mL, pH 7.5) at least 2–3 times greater than those employed in the NMR work (17–25 mg/mL, pH 7.0). Gronenborn et al. (1989) also suggest that the protein undergoes a conformational change (although not characterized) near pH 7.8. Although we observed no evidence of a conformational transition in either Mu or D108 Ner between pH 7.0 and 7.5, it is conceivable that such a transition may be concentration dependent, thus accounting for the observed difference. Conformational flexibility of the protein is consistent with the increase in α-helicity observed upon binding to the *ner* operator.

2. Base-Specific Interactions in the D108 Ner:DNA Complex. The pattern of interactions between D108 Ner and *ner* operator suggested by the present Raman experiments is different from that observed previously for λ repressor–operator interaction (Benevides et al., 1991a,b). Although both Ner:DNA and the λ repressor complex exhibit a Raman band shift characteristic of guanine 7N interactions, we find no evidence for D108 Ner side-chain interactions with either guanine 6-C=O or thymine 5-CH_3 groups of the 61-bp operator. In contrast, such interactions are prominently revealed in the Raman spectrum of the λ repressor complex. The absence of observable perturbations in the Ner repressor complex may be due in part to the greater surplus of nonperturbed DNA sites in the larger *ner* operator.

The present findings support chemical and enzymatic footprinting studies (Kukolj et al., 1989a), which suggest that recognition in D108 Ner is via the major groove and leave open the question of the configuration of the DNA double helix in the complex. The relatively high α-helix content of D108 Ner is consistent with a model for the complex in which the recognition scaffold is α-helical.

3. DNA Tertiary Structure in the D108 Ner:DNA Complex. The Raman spectra indicate that binding of D108 Ner perturbs the *ner* operator backbone more extensively than in the case of λ repressor–operator interactions, despite the 3-fold greater size of the *ner* operator sequence (Benevides et al., 1991a,b). In the λ complex, it is known from X-ray analysis that the operator is only slightly bent at the ends. The observed small perturbations to Raman markers of the B DNA backbone in the solution complex of λ repressor (Benevides et al., 1991a,b) are in accord with the crystal structure. The more extensive perturbations to Raman markers of the B DNA backbone in the D108 Ner:DNA complex are consistent with more significant modifications of DNA tertiary structure, involving substantial changes in helical twist or bending of DNA.

Kukolj et al. (1989a) have demonstrated that the *ner*-binding site for D108 Ner includes the two 11-bp inverted repeats shown in Figure 1. Methylation protection experiments show that adenines A(+21) and A(–22) exhibit enhanced reactivity following Ner binding, while guanines G(+22) and G(–23) show reduced reactivity. We speculate that these residues, which are located within the 11-bp inverted repeats, could define a bend in the D108 Ner:DNA complex. In support of this hypothesis, we note the following. The adenines exhibiting enhanced methylation are part of the sequence CGTGA, which is homologous with the statically bent sequence TGTGA in the DNA complex of the catabolite gene activator protein (CAP). CAP-induced DNA bending is associated with kinks occurring in the conserved TGTGA sequence (Schultz et al., 1991). The plausibility of Ner-induced kinks at TG steps in the *ner* operator is supported by additional similarities between the Ner- and CAP-binding sequences. Inspection of the two operators reveals the following extended homology:

```
CAP Consensus Sequence   TTGTGAxxTxxxTCAxA
ner Sequence             CCGTGAGCTACTTTATA
```

The homology between the above sequences is striking. If interchange of C for T is allowed, the CAP consensus sequence is matched exactly. Without pyrimidine interchange, it is still possible to match 8 of 11 conserved bases. Such a close correspondence between the CAP consensus sequence and *ner* sequence supports the notion that structural similarities exist in the modes of protein binding, viz., by induction of a bend in the DNA operator. This would be consistent with the present Raman spectroscopic results, previous footprinting studies (Kukolj et al., 1989a), and recent data showing that the two Ner proteins and their *E. coli* homologue (Nlp) can complement some *crp* mutants of *E. coli* for *crp* function (Autexier & DuBow, 1992). We also note that localized kinks postulated at the TG base step in each of the 11-bp inverted repeats coincide with the transcriptional start sites for both the Pe and Pc promoters (Kukolj & DuBow, 1992). Additional evidence for the role of GTG/CAC sequences as protein-inducible bending loci has been noted by several groups (Donlan & Lu, 1992; Frantz & O'Halloran, 1990; McNamara et al., 1990).

The DNA-binding sites of Ner and CAP, despite sequence homology, are constructed quite differently. The TG/AC steps, which constitute the sites of CAP-induced kinking (45°), are separated by 11 or 13 bp, depending upon whether the AT-rich spacer region is, respectively, 6 or 8 bp in length. For *ner*, the TG/AC pairs are separated by 22 bp (Figure 1). In order to properly orient the two TG/AC steps with respect to bound Ner, the intervening 22-bp segment must be underwound to achieve an average winding angle of 31.3°. Evidence of similar underwinding in the CAP system has been described recently (Barber et al., 1993). Underwinding of *ner* in the D108 Ner:DNA complex would also place the TATA sequence of the spacer region so that its major groove faces the repressor. Two models exhibiting these features are shown in Figure 6. Significant characteristics of these models are

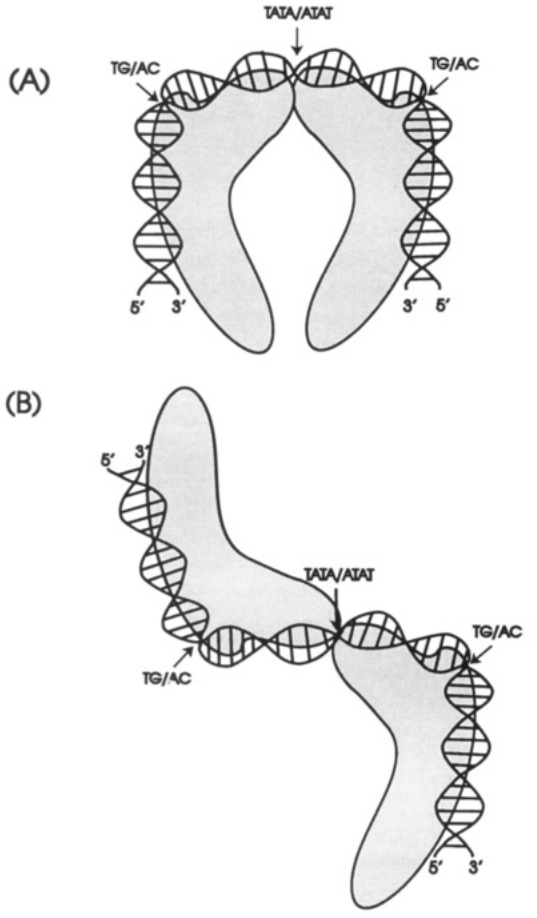

FIGURE 6: Models proposed for the D108 Ner:DNA complex. The cartoon depicts planar projections of the complex in which concerted bending of the 55-bp *ner* operator at the central TATA domain and at both adjacent TG steps leads to either U-shaped (A) or S-shaped (B) projections. Both planar and nonplanar configurations are consistent with the experimental results.

the central TATA/ATAT hinge, which is considered the most easily distorted DNA base sequence (Breslauer et al., 1986), and the two symmetry-related TG/AC steps. Distortion of the complex at these DNA junctures would allow for either planar or nonplanar configurations of the complex. The precise three-dimensional structure would depend upon the nature and magnitude of perturbations in the helix tilt, roll, and winding angles.

An average winding angle near 31° is not unusal for B DNA. In the cocrystal structure of λ repressor (Beamer & Pabo, 1992), seven of 18-bp steps have helical twists of less than 32°, with the lowest value near 21°. The overall structure of the DNA remains in the B form. Some studies have proposed a transition to A DNA in the spacer region to explain a change in CD spectra upon CAP binding to its operator (Ivanov et al., 1993; Barber et al., 1993). However, the present Raman data suggest that if DNA underwinding occurs in the Ner complex, it is accomplished without generating the C3′-*endo* nucleoside conformers characteristic of A DNA.

Although the available data are consistent with repressor-induced bending of B DNA, direct evidence of bent DNA in the complex has yet to be obtained. Other structural models consistent with the experimental results can also be envisioned, including the unwinding of DNA segments without appreciable bending of the double helix.

4. Comparison with Other Protein Sequences. The highly α-helical secondary structures indicated by the Raman amide markers of D108 and Mu Ner (Figure 3) suggest the likelihood of helix–turn–helix (HTH) recognition motifs, similar to those in other DNA repressors. Following is a sequence alignment of D108 and Mu Ner, which indicates significant homology with CAP and λ repressor sequences, using the criteria proposed by Brennan and Matthews (1989). For both D108 and Mu Ner, these sequences are predicted to favor HTH secondary structure (Garnier et al., 1978), consistent with the X-ray structures of CAP, cI, and Cro repressors (Steitz, 1990) and the NMR structure of Mu Ner (Gronenborn et al., 1989).

	Helix							Turn			Helix									
	1	2	3	4	5	6	7	8	9	10	11	12	13	14	15	16	17	18	19	20	21
CAP	168-T	R	Q	E	I	G	Q	I	V	G	C	S	R	E	T	V	G	R	I	L	K
D108	27-S	L	A	E	L	G	R	S	N	H	L	S	S	S	T	L	K	N	A	L	D
Mu	25-S	L	S	A	L	S	R	E	F	G	Y	A	P	T	T	L	A	N	A	L	E
cI	32-S	Q	E	S	V	A	D	K	M	G	M	G	Q	S	G	V	G	A	L	F	N
Cro	15-G	Q	T	K	T	A	K	D	L	G	V	Y	Q	S	A	I	N	K	A	I	N

The similarity score, which measures the relatedness of two different sequences, was calculated for each pair of sequences here by the method of McLachlan (1978). The similarity scores between D108 and Mu Ner (5.4), between cI and Cro repressors (4.4), and between either D108 or Mu Ner and CAP (4.2) are indicative of significant relatedness. Unrelated protein sequences exhibit much lower similarity scores (≈3.0).

SUMMARY

Present and previous experimental results suggest a greatly perturbed tertiary structure for the *ner* operator when bound by the D108 Ner repressor. Analysis of the DNA sequence and comparison with studies of other nucleoprotein complexes favor a model for the D108 Ner:DNA complex containing statically bent (or similarly altered) B DNA, in which the two GTG/CAC triplets are the likely loci for protein-induced operator bending. The central TATA/ATAT sequence, which is thermodynamically the most favorably bent 4-bp sequence, is also presumed to bend as shown in Figure 6 to facilitate the extensive protection observed in footprinting studies. Homologies among the amino acid sequences of Ner repressors (D108 and Mu), λ repressors (cI and Cro), and CAP further support the notion that the DNA-binding domains of the Ner repressors utilize an HTH module for DNA binding.

Comparison of the present Raman difference spectra with those obtained previously on λ cI repressor–operator complexes (Benevides et al., 1991a,b, 1994) shows that the Raman signatures of the two kinds of complexes are unique and easily distinguished. In view of the minimal degree of DNA bending induced upon binding of λ repressor, these results suggest that the Raman fingerprint may serve as a convenient method for distinguishing the degree of protein-induced bending in a DNA sequence to which the protein is bound.

ACKNOWLEDGMENT

We thank Alfredo Staffa for technical assistance in the purification of Mu Ner.

REFERENCES

Allet, B., Payton, M., Mattaliano, R. J., Gronenborn, A. M., Clore, G. M., & Wingfield, P. T. (1988) *Gene 65*, 259–268.

Aubrey, K. L., & Thomas, G. J., Jr. (1991) *Biophys. J. 60*, 1337–1349.

Anderson, W. F., Ohlendorf, D. H., Takeda, Y., & Matthews, B. W. (1981) *Nature 290*, 754–758.

Autexier, C., & DuBow, M. S. (1992) *Gene 114*, 13–18.

Barber, A. M., Zhurkin, V. B., & Adhya, S. (1993) *Gene 130*, 1–8.
Beamer, L. J., & Pabo, C. O. (1992) *J. Mol. Biol. 227*, 177–196.
Benevides, J. M., Wang, A. H.-J., van der Marel, G. A., van Boom, J. H., Rich, A., & Thomas, G. J., Jr. (1984) *Nucleic Acids Res. 12*, 5913–5925.
Benevides, J. M., Wang, A. H.-J., Rich, A., Kyogoku, Y., van der Marel, G. A., van Boom, J. H., & Thomas, G. J., Jr. (1986) *Biochemistry 25*, 41–50.
Benevides, J. M., Weiss, M. A., & Thomas, G. J., Jr. (1991a) *Biochemistry 30*, 4381–4388.
Benevides, J. M., Weiss, M. A., & Thomas, G. J., Jr. (1991b) *Biochemistry 30*, 5955–5963.
Benevides, J. M., Stow, P. L., Ilag, L., Incardona, N. L., & Thomas, G. J., Jr. (1991c) *Biochemistry 30*, 4855–4863.
Benevides, J. M., Weiss, M. A., & Thomas, G. J., Jr. (1994) *J. Biol. Chem. 269*, 10869–10878.
Bolotina, I. A., Kurochkin, A. V., & Kirpichnikov, M. P. (1983) *FEBS Lett. 155*, 291–293.
Brennan, R. G., & Matthews, B. W. (1989) *J. Biol. Chem. 264*, 1903-1906.
Brennan, R. G., Roderick, S. L., Takeda, Y., & Matthews, B. W. (1990) *Proc. Natl. Acad. Sci. U.S.A. 87*, 8165–8169.
Breslauer, K. J., Frank, R., Blöcker, H., & Marky, L. A. (1986) *Proc. Natl. Acad. Sci. U.S.A. 83*, 3746–3750.
Chen, M. C., & Lord, R. C. (1974) *J. Am. Chem. Soc. 96*, 4750–4752.
Clarke, N. D., Beamer, L. J., Goldberg, H. R., Berkower, C., & Pabo, C. O. (1991) *Science 254*, 267–270.
Donlan, M. E., & Lu., P. (1992) *Nucleic Acids Res. 20*, 525–532.
Erfurth, S. C., & Peticolas, W. L. (1975) *Biopolymers 14*, 247–264.
Frantz, B., & O'Halloran, T. V. (1990) *Biochemistry 29*, 4747–4751.
Garcia, J. A., Ou, S.-H. T., Wu, F., Lusis, A. J., Sparkes, R. S., & Gaynor, R. B. (1992) *Proc. Natl. Acad. Sci. U.S.A. 89*, 9372–9376.
Garnier, J., Osguthorpe, D. J., & Robson, B. (1978) *J. Mol. Biol. 120*, 97–120.
Giulian, G. G., Shanahan, M. F., Graham, J. M., & Moss, R. L. (1985) *Fed. Proc. 44*, 686.
Gronenborn, A. M., Wingfield, P. T., & Clore, G. M. (1989) *Biochemistry 28*, 5081–5089.
Harada, I., Miura, T., & Takeuchi, H. (1986) *Spectrochim. Acta 42A*, 307–312.
Harrison, S. C., & Aggarwal, A. K. (1990) *Annu. Rev. Biochem. 59*, 933–969.
Harshey, R. M. (1988) in *The Bacteriophages* (Calender, R., Ed.) Vol. 1, pp 193–234, Plenum Press, New York.
Hartman, K. A., Lord, R. C., & Thomas, G. J., Jr. (1973) in *Physicochemical Properties of Nucleic Acids* (Duchesne, J., Ed.) Vol. 2, pp 1–89, Academic Press, New York.
Heinemann, U., Lauble, H., Frank, R., & Blöcker, H. (1987) *Nucleic Acids Res. 15*, 9531–9550.
Ivanov, V. I., Minchenkova, L. E., Chernov, B. K., McPhie, P., Ryu, S., Garges, S., Barber, A. M., Zhurkin, B., & Adhya, S. (1993) *J. Biomol. Struct. Dyn. 10*, a80.
Jordan, S. R., & Pabo, C. O. (1988) *Science 242*, 893–899.
Kosturko, L. D., Daub, E., & Murialdo, H. (1989) *Nucleic Acids Res. 17*, 317–334.
Koudelka, G. B. (1991) *Nucleic Acids Res. 19*, 4115–4119.
Kukolj, G., & DuBow, M. S. (1992) *J. Biol. Chem. 267*, 17827–17835.
Kukolj, G., Tolias, P. P., Autexier, C., & DuBow, M. S. (1989a) *EMBO J. 8*, 3141–3148.
Kukolj, G., Tolias, P. P., & DuBow, M. S. (1989b) *FEBS Lett. 244*, 369–375.
Lahm, A., & Suck, D. (1991) *J. Mol. Biol. 222*, 645–667.
McClarin, J. A., Frederick, C. A., Wang, B.-C., Greene, P., Boyer, H. W., Grable, J., & Rosenberg, J. M. (1986) *Science 234*, 1526–1541.
McLachlan, A. D. (1971) *J. Mol. Biol. 61*, 409–424.
McNamara, P. T., Bolshoy, A., Trifonov, E. N., & Harrington, R. E. (1990) *J. Biomol. Struct. Dyn. 8*, 529–538.
Miura, T., Takeuchi, H., & Harada, I. (1988) *Biochemistry 27*, 88–94.
Miura, T., Takeuchi, H., & Harada, I. (1989) *J. Raman Spectrosc. 20*, 667–671.
Mizuuchi, M., Weisberg, R. A., & Mizuuchi, K. (1986) *Nucleic Acids Res. 14*, 3813–3825.
Morrisey, J. M. (1981) *Anal. Biochem. 117*, 307–310.
Nishimura, Y., & Tsuboi, M. (1986) in *Spectroscopy of Biological Systems, Advances in Spectroscopy* (Clark, R. J. H., & Hester, R. E., Eds.) Vol. 13, pp 177–232, Wiley, New York.
Nishimura, Y., Tsuboi, M., Sato, T., & Akoi, K. (1986) *J. Mol. Struct. 146*, 123–153.
Olson, W. K. (1982) *Nucleic Acids Res. 10*, 777–787.
Pabo, C. O., & Lewis, M. (1982) *Nature 298*, 443–447.
Pato, M. L. (1989) in *Mobile DNA* (Berg, D. E., & Howe, M. M., Eds.) pp 23–52, ASM Press, Washington, D.C.
Prescott, B., Steinmetz, W., & Thomas, G. J., Jr. (1984) *Biopolymers 23*, 235–256.
Priess, H., Kamp, D., Kahmann, R., Bräuer, B., & Delius, H. (1982) *Mol. Gen. Genet. 186*, 315–321.
Sargent, D., Benevides, J. M., Yu, M.-H., King, J., & Thomas, G. J., Jr. (1988) *J. Mol. Biol. 199*, 491–502.
Schultz, S. C., Shields, G. C., & Steitz, T. A. (1991) *Science 253*, 1001–1007.
Schumacher, R., Buck, F., & Ruterjans, H. (1989) *Nucleic Acids Res. 17*, 5097–5107.
Sczakiel, G., Wittinghofer, A., & Tucker, J. (1987) *Nucleic Acids Res. 15*, 1878.
Sengupta, P. K., & Krimm, S. (1987) *Biopolymers 26*, S99–S107.
Siamwiza, M. N., Lord, R. C., Chen, M. C., Takamatsu, T., Harada, I., Matsuura, H., & Shimanouchi, T. (1975) *Biochemistry 14*, 4870–4876.
Small, E. W., & Peticolas, W. L. (1971) *Biopolymers 10*, 1377–1416.
Steitz, T. A. (1990) *Q. Rev. Biophys. 23*, 205–280.
Thomas, G. A., & Peticolas, W. L. (1983) *J. Am. Chem. Soc. 105*, 993–996.
Thomas, G. J., Jr., & Agard, D. A. (1984) *Biophys. J. 46*, 763–768.
Thomas, G. J., Jr., & Wang, A. H.-J. (1988) *Nucleic Acids Mol. Biol. 2*, 1–30.
Thomas, G. J., Jr., Prescott, B., & Day, L. A. (1983) *J. Mol. Biol. 165*, 321–356.
Thomas, G. J., Jr., Prescott, B., Benevides, J. M., & Weiss, M. A. (1986) *Biochemistry 25*, 6768–6778.
Thomas, G. J., Jr., Prescott, B., & Urry, D. W. (1987) *Biopolymers 26*, 921–934.
Tolias, P. P., & DuBow, M. S. (1985) *EMBO J. 4*, 3031–3037.
Wartell, R. M., & Harrell, J. T. (1986) *Biochemistry 25*, 2664–2671.